Magnetic Soft Continuum Robots for Minimally Invasive Surgery. Trends and Simulation Models

Shuangshuang MENG[1], Abdolrahim SALEHNIA[1], Caroline BALLOY[1], Brahim TAMADAZTE[2], Mokrane BOUDAOUD[2], Fahmi BEDOUI[1], Arnaud HUBERT[1]

[1] Laboratoire Roberval, Université de Technologie de Compiègne, Centre de recherche de Royallieu, CS 60319, 60203 Compiègne, Cedex, France.

[2] Sorbonne Université, CNRS UMR 7222, INSERM U1150, ISIR, F-75005, Paris, France.

ABSTRACT – This paper studies the mechanism, modelling, and applications of deformable magnetized structures under external magnetic fields. These structures, known as "magnetic soft continuum robots" (MSCRs), have become increasingly interesting because they allow advances in the field of intra-corporeal navigation and minimally invasive surgery. Several scientific and technological challenges arise in the design, modelling and control of this new family of soft robots. This paper investigates the modelling of such mechanisms both analytically and numerically. Finally, a series of simulations including various magnetic fields and magnetization configurations of the proposed robotic system are carried out. The preliminary results demonstrate the relevance of this type of robot, and provide a new perspective for the design and optimization of this robot in some targeted applications.

Keywords – Magnetic Soft Continuum Robots, Magneto-Mechanical Behavior, Numerical and Analytical Models, Minimally Invasive Surgery.

1. INTRODUCTION

Small-scale soft continuum robots are increasingly becoming essential in several robotics disciplines, especially in medical applications, e.g., minimally invasive surgery (MIS) [1, 2]. Particularly, compared to traditional surgery for patients with cardiovascular disease, MIS allows significantly reduce complications, shorter hospital stays, and faster recovery times [3, 4, 5]. Therefore, numerous continuum robot concepts have been introduced in the market, presenting a diverse set of minimally invasive therapeutic and diagnostic procedures that offer enhanced patient safety [6]. For instance, a passive guidewire and catheter with a pre-shaped tip are commonly utilized, which are manually maneuvered under fluoroscopy imaging. However, this kind of passive mechanisms is often constrained by various factors such as low steerability in complex vasculatures, difficulty in accessing small branches, long operation times, and the increased accumulation of radiation exposure for both patients and physicians [7]. To tackle these issues, considerable endeavours have been undertaken to investigate the feasibility of robot-assisted minimally invasive treatments that can be operated from a remote location. On the other hand, scaling down tendon-driven continuum robots [8] with antagonistic pairs of wires to submillimeter diameters is challenging due to the rising complexities in the fabrication process as the components become smaller [9, 10].

Magnetic Soft Continuum Robots (MSCRs) are recently investigated due to their numerous benefits such as better controllability, enhanced dynamic behavior, and safety. These robots have the potential to overcome the limitations of traditional robots, including tether-free actuation, instabilities with multiple passive degrees of freedom (DoF), and miniaturization. These advantages make the applications of robots in MIS procedures become more promising [13, 14, 12, 11]. MSCRs have initially been fabricated by incorporating discrete permanent magnets into the distal portion. However, the size of the embedded magnets required to generate deflection under applied magnetic fields has limited their fabrication to larger scales [1, 15, 16]. Additionally, the use of such rigid magnets at submillimeter scales has led to concerns about the potential for breakage and clinical problems, as evidenced by the recall of several magnet-tipped micro-guidewires seeking US Food and Drug Administration (FDA) market approval [17]. A solution to this challenge has emerged, particularly with the breakthrough achieved in recent years by Zhao *et al.* [18, 19], which first proposed using a Hard-magneto-active composite to build a robot's structure. This robot is composed of soft polymers with embedded hard-magnetic particles as distributed actuation sources, which is able to produce large-scale elastic deflections through magnetic torques and/or forces generated from the intrinsic magnetic dipoles under the influence of the external magnetic field. This mechanical design allows better steering and navigational capabilities at much smaller scales, which differentiate them from previously continuum robots. Based on this work, many teams around the world have started to develop simulation tools for design (based on analytical and FEM models) and applications of such active structures, referred to as *hard-magnetic soft materials* [18, 20, 21, 22]. Good recent reviews on these topics can be found in [11, 23].

This paper focuses primarily on the modelling aspect, including analytical and numerical simulations for hard-magnetic MSCRs. Its main purpose is to study the mechanical deflections of robot bodies under various designs (internal properties and topologies) and external magnetic fields, the objective being to facilitate decision-making for the design of these devices.

2. MODELING MAGNETIC SOFT CONTINUUM ROBOTS

2.1. Analytical Modelling

The material of MSCRs is a composite of soft polymer embedded with hard-magnetic particles (NdFeB). They are mainly manufactured from the beam topologies (slender geometry and planar motion), as the example shown in Fig. 1. Therefore, a Kirchhoff assumption can be applied in their analytical models, considering a negligible stretch and a dominating bending deformation. The total Helmholtz free energy U of a hard-magnetic beam is proposed by [18] and it consists of two parts: a bending energy U^b and a magnetic potential U^m. According to the Euler beam assumption [24], the bending energy is given in terms of the curvature of the beam centerline, $\kappa = \theta' = \frac{\partial \theta}{\partial s}$ with s the curvilinear coordinate, and θ the tangent angle:

$$U^b = \frac{1}{2}\int_0^L EI{\theta'}^2 ds, \tag{1}$$

where I is the area moment of inertia of the beam's cross-section and E is the Young modulus. The magnetic potential is asso-

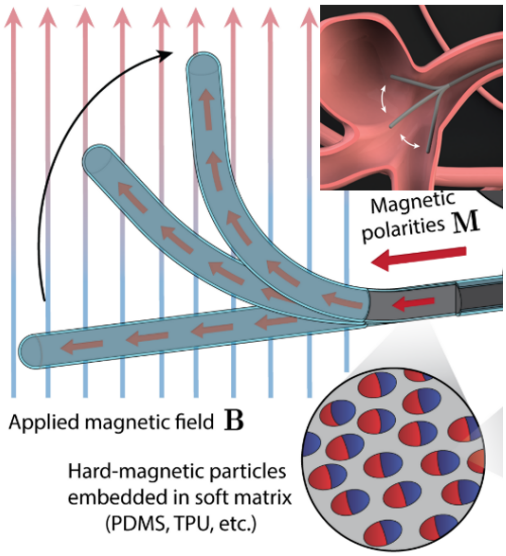

Figure 1. One of the robotic prototypes from [19] and its potential use in navigating in cerebrovascular structures.

ciated with the work done by magnetic body torque to align the magnetization of the robot body, together with the magnetic body force. Based on [21], the 3D magnetic potential can be reduced to 1D affected on the beam centerline by considering only the contribution of the rotation matrix $\mathbf{R}$ to the magnetic energy (deformation matrix $\mathbf{F} = \mathbf{R}$ under the condition of incompressibility):

$$U^m = \int_V -\mathbf{RM} \cdot \mathbf{B}^{applied} dV, \tag{2}$$

with $\mathbf{M}$ the magnetization of the robot body and $\mathbf{B}^{applied}$ the externally applied magnetic field. At a stationary/equilibrium condition, the first variation of the total energy must vanish for any arbitrary variation in the configuration, i.e. $\delta U = 0, \forall\, \delta\theta$:

$$\delta U = U(\theta + \delta\theta) - U(\theta) = \delta U^b + \delta U^m = 0, \tag{3}$$

Let us consider an external field $\mathbf{B}^{applied}$ that changes linearly with space location, such that it can be written as follows:

$$\mathbf{B}^{applied} = \mathbf{B}^c + (\nabla \mathbf{B}^a)(\mathbf{x} - \mathbf{x}_0) \tag{4}$$

and a boundary condition such that $\theta' \delta\theta|_0^L = 0$. Equations (1) and (2) can be integrated to give the equilibrium equations of the hard-magnetic beams:

$$EI\theta^{"} + At_z^m - A\sin\theta \int_s^L f_x^m ds' + A\cos\theta \int_s^L f_y^m ds' = 0 \tag{5}$$

Three force contributions appear in this equation: a torque around the z axis and two forces along the x and y axis:

$$\begin{cases} t_z^m = [\mathbf{RM} \times \mathbf{B}^{applied}] \cdot \mathbf{e}_z \\ (f_x^m, f_y^m) = \mathbf{f^m} = (\nabla \mathbf{B^a})^T (\mathbf{RM}) \end{cases} \tag{6}$$

The difficulty of solving (5) depends largely on the configurations of the external field $\mathbf{B}$ and the configuration of field $\mathbf{M}$. The authors in [18, 7] propose the semi-analytical solutions for a constant magnetic field with varied field $\mathbf{M}$. The `Matlab bvp5c` solver can also be used to solve the more general integro-differential equation (5), which models the deformations of MSCRs under both torque and force.

2.2. *FEM implementation*

In Finite Elements Modelling (FEM) formulations, a 3D continuum body of volume V bounded by surface S in its current configuration is considered as the MSCR body. Combined with boundary conditions $\mathbf{t}$, traction forces at S_t, the equilibrium equation under the Principle of Virtual Work (PVW) can be written as:

$$\int_V \boldsymbol{\sigma}^T : \frac{\partial \delta \mathbf{u}}{\partial \mathbf{x}} dV = \int_{S_t} \mathbf{t} \cdot \delta \mathbf{u}\, dS + \int_V \mathbf{f}^m \cdot \delta \mathbf{u}\, dV \tag{7}$$

here, in the left term, the total Cauchy stress consists of two parts: $\sigma = \sigma^e + \sigma^m$. The elastic part σ^e is determined by a Neo-Hookean constitutive model proposed by [18], and is derived from the first Piola–Kirchhoff stress $\mathbf{P}^e = J\sigma^e \mathbf{F}^{-\mathbf{T}}$. J is determinant of $\mathbf{F}$. The magnetic component of the Cauchy stress is:

$$\sigma^m = -\mathbf{m} \otimes \mathbf{B}^a \tag{8}$$

where $\mathbf{m} = J^{-1}\mathbf{FM}$ is the remanent magnetization in the current configuration. From the above equilibrium equation, we can identify the magnetic body force because of the existence of a gradient magnetic field:

$$\mathbf{f}^m = (\nabla \mathbf{B}^a)^T \mathbf{m}, \tag{9}$$

Subsequently, the weak form at the element level, considering the volume of the element V^{element} and the surface S_t^{element} subjected to traction forces $\mathbf{t}$, can be represented as:

$$\int_{V^{\text{element}}} \boldsymbol{\sigma}^T : \frac{\partial \delta \mathbf{v}}{\partial \mathbf{x}} dV = \int_{S_t^{\text{element}}} \mathbf{t} \cdot \delta \mathbf{v}\, dS + \int_{V^{\text{element}}} \mathbf{f}^m \cdot \delta \mathbf{v}\, dV \tag{10}$$

The residual of the element at the nodes, considering the approximated displacement field $\mathbf{u} = \sum_{I=1}^n \mathbf{u}^I N^I$ and virtual velocity field $\delta \mathbf{v} = \sum_{I=1}^n \delta \mathbf{v}^I N^I$, where N^I represents the shape function for node number $I = 1, 2, \ldots, n$, can be expressed as:

$$(\mathbf{R_u})^I = -\int_{V^{\text{element}}} \boldsymbol{\sigma}^T \frac{\partial N^I}{\partial \mathbf{x}} dV + \int_{V^{\text{element}}} N^I \mathbf{f}^m\, dV + \int_{S_t^{\text{element}}} N^I \mathbf{t}\, dS, \tag{11}$$

Hence, to find the nodal displacements at equilibrium, the equation $(\mathbf{R_u})^I = 0$ is solved using the Newton-Raphson method. This iterative method requires updating the intermediate solution in each iteration by calculating the Jacobian of the element's residual; *i.e.* ,

$$(\mathbf{K_{uu}})^{IJ} = -\frac{\partial (R_\mathbf{u})^I}{\partial \mathbf{u}^J}, \tag{12}$$

where $I, J = 1, 2, \cdots, n$ are node numbers in an element.

The expression of $(\mathbf{K_{uu}})^{IJ}$ is provided in the following by [21] who extended it to the case with the gradient magnetic field:

$$\begin{aligned} [(\mathbf{K_{uu}})^{IJ}]_{ij} = \int_{V_{\text{element}}} (& J^{-1} \frac{\partial N^I}{\partial x_k} \frac{\partial P^e_{im}}{\partial \mathbf{F}_{jn}} \mathbf{F}_{km} \mathbf{F}_{ln} \frac{\partial N^J}{\partial x_I} \\ & - J^{-1} \frac{\partial \mathbf{N}^I}{\partial x_k} \mathbf{F}_{kl} \mathbf{M}_I \nabla \mathbf{B}^a_{ij} N^J \\ & - J^{-1} \mathbf{N}^I \mathbf{F}_{kl} \mathbf{M}_I \nabla \mathbf{B}^a_{ij} \frac{\partial N^J}{\partial x_k}) dV \end{aligned} \tag{13}$$

where $i, j = 1, 2, 3$ denote the ith and jth spatial coordinates. In this Equation, the final two terms arise from the field gradient$\nabla \mathbf{B}^a$. These terms, however, become negligible when the fields are uniform and effectively disappear. The FE formulation was implemented using the `Abaqus` FE software. The procedure utilizes an eight-noded brick user-element, more details seen in [20, 21].

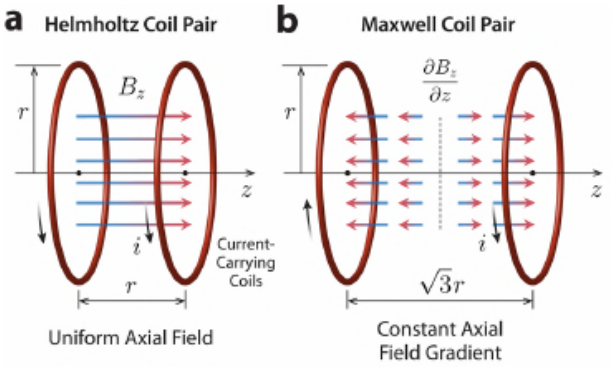

Figure 2. Coil arrangement: (a) Helmholtz coil pair, (b) Maxwell coil pair [11].

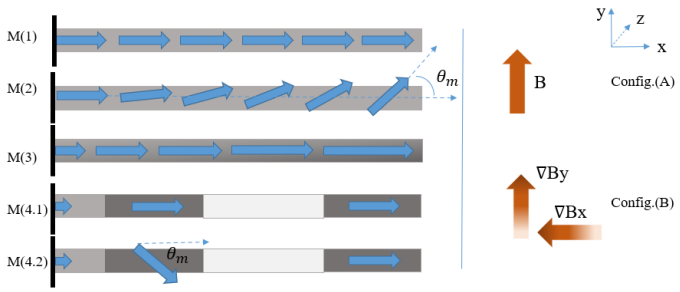

Figure 3. Left side: different magnetization $\mathbf{M}$ in the robot bodies. The sizes and directions of the blue arrows represent the magnitude and direction of $\mathbf{M}$. The geometrical and mechanical parameters are taken from [7] (length L=40mm, diameter D=$L/20$, and $\mathbf{M}$=$\mathbf{M}_0\phi$, $\mathbf{M}_0$=640kA/m). Right side: a uniform *Config.(A)* and a constant gradient field *Config.(B)* with $\nabla\mathbf{B}_x = -0.5\nabla\mathbf{B}_y$ (see [21] for more details).

3. SIMULATION RESULTS AND DISCUSSION

3.1. *Description of the Magnetic field and Magnetization*

As noted previously, performance of MSCRs rely largely on the magnetic fields and magnetization distributions. Several configurations will be considered in the following. As discussed in [21], two magnetic fields can be generated by two identical multi-turns electromagnetic coils arranged as Helmholtz or Maxwell pairs (Fig. 2). In this paper, we focus on two configurations referred to *Config. (A)* (constant magnetic field $\mathbf{B}^c = (0 \quad B_y \quad 0)^T$) and *Config. (B)* (constant gradient magnetic field $\nabla\mathbf{B}^a = (\nabla B_x \quad \nabla B_y \quad 0)^\top$) as depicted on the right side of Fig. 3.

The left side of Fig. 3 presents five distributions of $\mathbf{M}$ into the MSCRs. The strength of $\mathbf{M}$ is controlled by the volume fraction ϕ of hard-magnetic particles mixed in the composite materials. The simulations can be carried out in cases with various combinations of magnetic fields and magnetization. Table 1 summarizes the cases already addressed in [21, 7], and newly investigated in this work (**v.1**, **v.2** and **v.3**).

Table 1. Configuration addressed in this paper ('X' means not already studied).

	M(1)	**M(2)**	**M(3)**	**M(4.1)**	**M(4.2)**
Config. (A)	[7], [21]	[21], **v.1**	[7]	[7], **v.2**	**v.2**
Config. (B)	[21]	[21]	**v.3**	X	X

3.2. *Examples of results for* Config. (A)

The *Config. (A)* corresponds to the case of the application of a constant external magnetic field (Helmholtz coil pair). This configuration only produces a torque into the beam that results in a bending motion around the $z-axis$.

Figure 4 shows the results of **v.1** which consists of two values of θ_m in $\mathbf{M}(2)$. The agreements between analytical and FEM analysis confirm their suitability for computing the deformations of MSCRs with non-homogeneous magnetization distribution. Moreover, we demonstrate that a magnetization with a varied orientation enhances the possibilities of beam deformation in terms of the curvature along the robot body.

The second example (**v.2**) highlights the performance of $\mathbf{M}(4.1)$ that was optimized in [7] to increase its workspace by selecting different magnitudes of $\mathbf{M}$ into multiple segments of the robot body. Because **v.1** shows the importance of a varied direction θ_m in the beam deformations, a configuration $\mathbf{M}(4.2)$ is tested by changing the orientation θ_m in one segment of the configuration $\mathbf{M}(4.1)$. A comparison about the deflections between $\mathbf{M}(4.1)$ and $\mathbf{M}(4.2)$ is shown in Fig. 5. It can be seen that the deflections are larger in $\mathbf{M}(4.2)$ than in $\mathbf{M}(4.1)$, especially in the range with a bigger strength of magnetic field $\mathbf{B}$. This result demonstrates that an optimization involving both the magnitude and direction of the magnetization of the robot body has great potential to produce a more effective workspace for MSCRs.

3.3. *Examples of results for* Config. (B)

The *Config. (B)* corresponds to the case of the application of a constant external magnetic gradient field (Maxwell coil pair). This configuration produces forces along the x and y axis such that extension deformation appears.

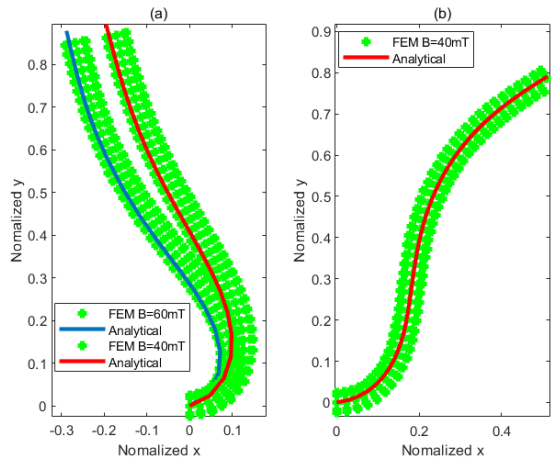

Figure 4. The **M(2)** magnetization distribution with *Config. (A)* for two cases: (a) is with $\theta_m = \frac{\pi}{2L}s$, (b) is with $\theta_m = \frac{3\pi}{2L}s - \frac{\pi}{2}$.

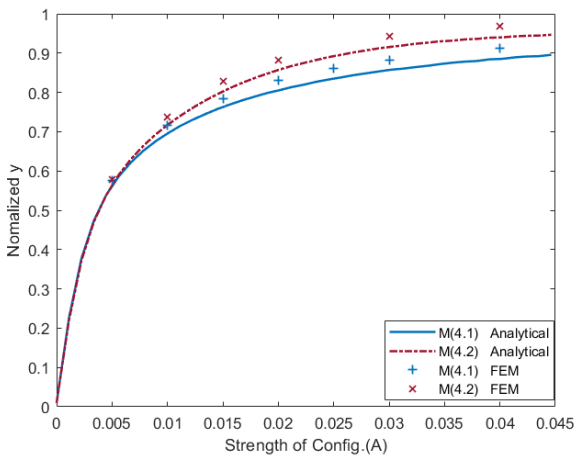

Figure 5. Comparison between **M(4.1)** and **M(4.2)** for *Config. (A)*.

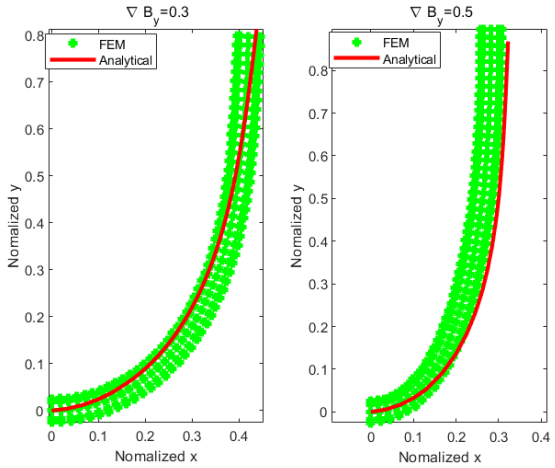

Figure 6. The **M(3)** magnetization with *Config. (B)* for $\phi = 0.4s/L$.

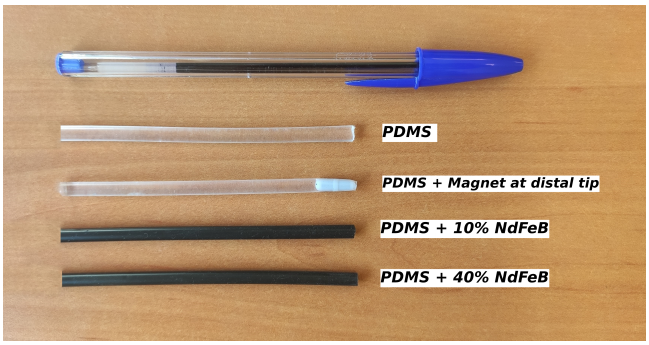

Figure 7. Examples of designed and manufactured magnetic soft continuum robot prototypes.

The last example (**v.3**) investigated the deflection of $\mathbf{M}(3)$ under the gradient field of *Config. (B)*. Figure 6 shows the results at two points with various strengths of the gradient fields. The matching between simulation results (using both analytical and FEM methods) confirms the adequacy of both methods to predict the deformation of robots with varied magnitude under a gradient field.

4. EXTENSION AND FUTURE WORKS

Based on these early modelling results, we are currently developing experimental prototypes. After testing several materials, we now use PDMS as the polymer base of the beam. Figure 7 shows photographs of our first prototypes: pure PDMS, PDMS mixed with NdFeB particles for $\phi = 0.1$ (10% of particles fraction) and $\phi = 0.4$ (40% of particles fraction). A prototype including a permanent magnet in the distal part is also manufactured. The samples with NdFeB particles are not yet magnetised but they will be as soon as we have access to a magnetisation equipment. The first experimental tests will be conducted after this magnetization procedure.

Currently, the estimation of forces applied to the beam after a contact with an external solid is also considered. Indeed, the estimation of contact forces between MSCR and biological matter is fundamental for medical applications and MIS procedures. Authors in [25, 26] have proposed some models for punctual contact. Particularly, [26] proposed an interesting design for specific contact conditions (a contact force limited to the 0.1 N to 0.4 N range in order to improve the procedural outcome of cardiac ablation). It should be noticed that these models do not consider distributed force along MSCR, which becomes important during the navigation of the robot in a specific vascellum with complex curvature or in the arteries with aneurysms. This is one of our next modelling objectives. In this way, we also work with robotics partners that already proposed some solutions to assist this estimation of force using visual feedback [27]. This work is currently proposed for a passive beam, and we want to extend these results to consider a hard magnetic continuum beam.

5. CONCLUSION

This article presents an analytical and FEM-based model to compute the deformations of MSCRs subject to various magnetic fields. The main objective of this work is to help decision-making for the design of these devices. The early obtained results demonstrated promising investigation paths, for instance considering the direction and magnitude of the magnetization in designing robots could improve greatly their performances. Nevertheless, because of the complexity of the magneto-mechanical coupling problem in composite materials with largely nonlinear deformations, these preliminary modeling results must be strengthened by further investigations.

Progress is currently being made on the fabrication of prototypes that will allow us to carry out the first experiments. We will then be able to start addressing the "real" robotics and control problems associated with these devices, beyond the "simple" simulation of their magneto-mechanical behavior.

6. AKNOWLEDGMENTS

This work was supported by *Alliance Sorbonne Universités* through funding of the “MagRobHealth” *Emergence Project*.

7. REFERENCES

[1] Edelmann, J., Petruska, A. J., Nelson, B. J. (2017). Magnetic control of continuum devices, International Journal of Robotics Research, Vol. 36(1).

[2] Zhou, C. et al. (2021), Ferromagnetic soft catheter robots for minimally invasive bioprinting, Nature Communications, Vol. 12.

[3] Kuan-Ming Chiu (2013), Minimally invasive cardiac surgery, Formosan Journal of Surgery, Vol. 46(6), pp 183-188.

[4] Schmitto JD, Mokashi SA, Cohn LH. (2010), Minimally-invasive valve surgery. J Am Coll Cardiol., 56(6), pp 455-62.

[5] Iribarne A, Easterwood R, Chan EY, Yang J, Soni L, Russo MJ, Smith CR, Argenziano M. (2011), The golden age of minimally invasive cardiothoracic surgery: current and future perspectives. Future Cardiol., 7(3), pp 333-46.

[6] H. Rafii-Tari, C. J. Payne, G.-Z. Yang (2014), Current and emerging robot-assisted endovascular catheterization technologies: A review. Ann. Biomed. Eng., Vol. 42, pp 697–715.

[7] Wang, L., Zheng, D., Harker, P., Patel, A. B., Guo, C. F., & Zhao, X. (2021). Evolutionary design of magnetic soft continuum robots. National Academy of Sciences of the United States of America, Vol. 118(21).

[8] T. Kato, I. Okumura, S.-E. Song, A. J. Golby, N. Hata (2015), Tendon-driven continuum robot for endoscopic surgery: Preclinical development and validation of a tension propagation model. IEEE/ASME Transactions on Mechatronics, Vol. 20, pp 2252–2263.

[9] Z. Li, L. Wu, H. Ren, H. Yu (2017), Kinematic comparison of surgical tendon-driven manipulators and concentric tube manipulators. Mech. Mach. Theory, Vol. 107, pp 148–165.

[10] Y.-H. Kim, Y.-J. Park, H. In, C. W. Jeong, K.-J. Cho (2016), Design concept of hybrid instrument for laparoscopic surgery and its verification using scale model test. IEEE/ASME Transactions on Mechatronics, Vol. 21, pp 142–153.

[11] Kim, Y., Zhao, X. (2022). Magnetic Soft Materials and Robots, Chemical Reviews, Vol. 122(5), pp 5317-5364.

[12] Wang, B., Kostarelos, K., Nelson, B. J., Zhang, L. (2021), Trends in Micro-/Nanorobotics: Materials Development, Actuation, Localization, and System Integration for Biomedical Applications. Adv. Mater., Vol. 33, 2002047.

[13] Hwang, J., Kim, Jy. & Choi, H. (2020), A review of magnetic actuation systems and magnetically actuated guidewire- and catheter-based micro-robots for vascular interventions, Intel Serv Robotics, Vol. 13, pp 1–14.

[14] Z. Yang, L. Zhang (2020), Magnetic actuation systems for miniature robots: A review. Adv. Intell. Syst., Vol. 2, 2000082.

[15] J. Sikorski, A. Denasi, G. Bucchi, S. Scheggi and S. Misra (2019), "Vision-Based 3-D Control of Magnetically Actuated Catheter Using BigMag—An Array of Mobile Electromagnetic Coils," in IEEE/ASME Transactions on Mechatronics, vol. 24(2), pp. 505-516.

[16] Jeon, S., Hoshiar, A.K., Kim, S. et al. (2018), Improving guidewire-mediated steerability of a magnetically actuated flexible microrobot. Micro and Nano Syst Lett, Vol. 6(15).

[17] U.S. Food and Drug Administration (FDA), Class 2 medical device recalls: Cronus endovascular guidewires (510(K) Number: K021363, FDA, 2004).

[18] Zhao, R., Kim, Y., Chester, S. A., Sharma, P., & Zhao, X. (2019). Mechanics of hard-magnetic soft materials. Journal of the Mechanics and Physics of Solids, Vol. 124, 244–263.

[19] Kim, Y., Parada G. A., Liu, S., Zhao, X. (2019). Ferromagnetic soft continuum robots, Science Robotic, Vol. 4.

[20] Wang, L., Kim, Y., Fei Guo, C., Zhao, X. (2020). Hard-magnetic elastica. Journal of the Mechanics and Physics of Solids, Vol. 142, 104045.

[21] Yan, D., Abbasi, A., Reis, P. M. (2022). A comprehensive framework for hard-magnetic beams: Reduced-order theory, 3D simulations, and experiments, International Journal of Solids and Structures, Vol. 257, 111319.

[22] Garcia-Gonzalez, D., & Hossain, M. (2021). Microstructural modelling of hard-magnetic soft materials: Dipole–dipole interactions versus Zeeman effect. Extreme Mechanics Letters, 48, 101382.

[23] Sergio Lucarini, S., Hossain, M., Garcia-Gonzalez, D. (2022). Recent advances in hard-magnetic soft composites: Synthesis, characterisation, computational modelling, and applications, Composite Structures, Vol. 279.

[24] Audoly B, Pomeau Y. (2010), Elasticity and geometry: from hair curls to the non-linear response of shells, Oxford University Press.

[25] Venkiteswaran V., Sikorski J., Misra S. (2019), Shape and contact force estimation of continuum manipulators using pseudo rigid body models, Mechanism and Machine Theory, Vol. 139, pp 34–45.

[26] Wang L., Fei Guo C., Zhao, X. (2022), Magnetic soft continuum robots with contact forces, Extreme Mechanics Letters, Vol. 51.

[27] Diezinger M. A.,Tamadazte B., Laurent G. (2022), 3D Curvature-Based Tip Load Estimation for Continuum Robots, IEEE Robotics and Automation Letters, Vol. 7(4).